NEURAL REGENERATION RESEARCH
www.nrronline.org

Research Article

# Pathological axonal enlargement in connection with amyloidosis, lysosome destabilization, and bleeding is a major defect in Alzheimer's disease

Hualin Fu[1, 2, 3, *], Jilong Li[1], Chunlei Zhang[1, 3], Guo Gao[1, 3], Qiqi Ge[2, 4], Xinping Guan[4, 5], Daxiang Cui[1, 3]

https://doi.org/10.4103/NRR.NRR-D-24-01440
Date of submission: November 18, 2024
Date of decision: February 21, 2025
Date of acceptance: March 17, 2025
Date of web publication: April 30, 2025

### From the Contents



### Graphical Abstract

***Hemorrhagic amyloidosis is associated with lysosome destabilizaiton, axonal enlargement, spheroid formation, and axon breaks in Alzheimer's disease (AD)***

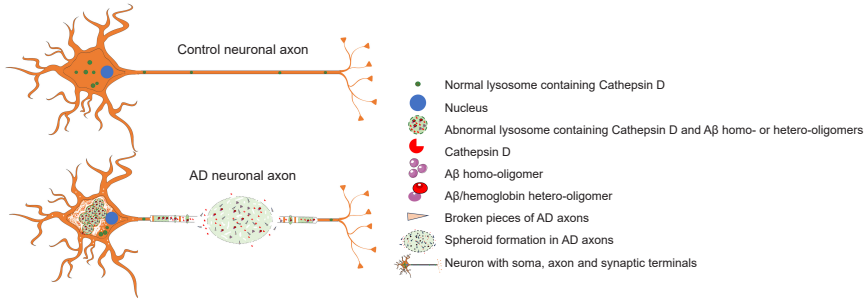


## Abstract

Alzheimer's disease is a multi-amyloidosis disease characterized by amyloid-β deposits in brain blood vessels, microaneurysms, and senile plaques. How amyloid-β deposition affects axon pathology has not been examined extensively. We used immunohistochemistry and immunofluorescence staining to analyze the forebrain tissue slices of Alzheimer's disease patients. Widespread axonal amyloidosis with distinctive axonal enlargement was observed in patients with Alzheimer's disease. On average, amyloid-β-positive axon diameters in Alzheimer's disease brains were 1.72 times those of control brain axons. Furthermore, axonal amyloidosis was associated with microtubule-associated protein 2 reduction, tau phosphorylation, lysosome destabilization, and several blood-related markers, such as apolipoprotein E, alpha-hemoglobin, glycosylated hemoglobin type A1C, and hemin. Lysosome destabilization in Alzheimer's disease was also clearly identified in the neuronal soma, where it was associated with the co-expression of amyloid-β, Cathepsin D, alpha-hemoglobin, actin alpha 2, and collagen type IV. This suggests that exogenous hemorrhagic protein intake influences neural lysosome stability. Additionally, the data showed that amyloid-β-containing lysosomes were 2.23 times larger than control lysosomes. Furthermore, under rare conditions, axonal breakages were observed, which likely resulted in Wallerian degeneration. In summary, axonal enlargement associated with amyloidosis, micro-bleeding, and lysosome destabilization is a major defect in patients with Alzheimer's disease. This finding suggests that, in addition to the well-documented neural soma and synaptic damage, axonal damage is a key component of neuronal defects in Alzheimer's disease.
**Key Words:** Alzheimer's disease; amyloid-β; amyloidosis; axonal enlargement; hemoglobin; hemorrhage; lysosome destabilization; neuropil thread; tau; Wallerian degeneration

## Introduction

The pathological hallmarks of Alzheimer's disease (AD) include senile plaques, neurofibrillary tangles, and neuritic dystrophy (Hardy and Higgins, 1992; Lane et al., 2018), the latter of which refers to the dystrophy of axons and dendrites. Previously, we identified cerebral microaneurysm rupture and hemorrhagic amyloid-β (Aβ) leakage as a pathological mechanism underlying senile plaque formation (Fu et al., 2023). However, the impact of chronic hemorrhagic leakage on other pathological phenotypes of AD, such as axonal dystrophy, is poorly understood. Previous studies have implicated both Aβ and tau phosphorylation in the axonal defects observed in AD (Cras et al., 1991; Tsai et al., 2004; Braak and Del Tredici, 2013; Blazquez-Llorca et al., 2017; Salvadores et al., 2020). The widespread axonal enlargement associated with Aβ deposition may significantly influence AD pathology. In natural animal species, axons with larger diameters have higher transduction speeds, as demonstrated in the squid giant axon (Hartline and Colman, 2007). However, in the case of AD, enlarged axons are not natural but pathological, and are filled with toxic Aβ, hemorrhagic proteins, and enlarged and destabilized lysosomes. In addition, lysosomal leakage can induce axonal structural damage and increase axolemmal permeability, which can further damage the myelin sheath. Both human and mouse studies have indicated that axon diameter increases with age and cognitive decline (Fan et al., 2019; Parandavar et al., 2024). Moreover, the velocity of action potential transmission is reduced in AD patients and AD-model transgenic mice (Gelman et al., 2020; Qian et al., 2022). Diffusion tensor imaging studies have also shown that structural damage and disconnection in the white matter are prominent in patients with AD (Fellgiebel and Yakushev, 2011; Chen et al., 2023). Therefore, axonal amyloidosis and enlargement in AD are likely linked to transduction velocity reduction and white matter damage phenotypes. In addition to the basic axonal enlargement phenotype of AD, spheroid formation is frequently

[1]Institute of Nano Biomedicine and Engineering, School of Sensing Science and Engineering, School of Electronic Information and Electrical Engineering, Shanghai Jiao Tong University, Shanghai, China; [2]Institute of Marine Equipment, Shanghai Jiao Tong University, Shanghai, China; [3]National Center for Translational Medicine, Shanghai Jiao Tong University, Shanghai, China; [4]Department of Automation, Shanghai Jiao Tong University, Shanghai, China; [5]The Key Laboratory of System Control and Information Processing, Ministry of Education, Shanghai, China
*Correspondence to: Hualin Fu, PhD, hfu@sjtu.edu.cn or 1010720220@qq.com.
https://orcid.org/0000-0002-0189-0282 (Hualin Fu)

*Funding:* *This study was supported by the National Natural Science Foundation of China, No. 81472235 (to HF); the Shanghai Jiao Tong University Medical and Engineering Project, Nos. YG2021QN53 (to HF), YG2017MS71 (to HF); the International Cooperation Project of the National Natural Science Foundation of China, No. 82020108017 (to DC); and the Innovation Group Project of the National Natural Science Foundation of China, No. 81921002 (to DC).*
*How to cite this article:* *Fu H, Li J, Zhang C, Gao G, Ge Q, Guan X, Cui D (2026) Pathological axonal enlargement in connection with amyloidosis, lysosome destabilization, and bleeding is a major defect in Alzheimer's disease. Neural Regen Res 21(2):790-799.*

observed. Previous studies have demonstrated that spheroid formation on axons also slows down the speed of action potential transduction (Kolaric et al., 2013; Yuan et al., 2022). Taken together, these findings provide strong evidence that patients with AD have serious axonal defects, with transduction speed decline as a central phenotype. Understanding how and to what extent Aβ deposition in enlarged axons impacts the function of the whole brain connectome requires large-scale quantitative analysis and *in vivo* animal and human studies. Therefore, in the current study, we analyzed the pathological phenotypes of the axons of AD brain tissues using immunohistochemistry, histochemistry, and fluorescent imaging methods to identify axonal defects linked to Aβ deposition.

## Methods

### Tissue sections

Frontal lobe paraffin tissue sections of AD patients were purchased from GeneTex (Irvine, CA, USA). Additionally, AD patient and control frontal lobe paraffin tissue sections were provided by the National Human Brain Bank for Development and Function, Chinese Academy of Medical Sciences, and Peking Union Medical College, Beijing, China. The study does not involve live human samples or clinical human experiments, and all experiment procedures were performed in accordance with the ethical standards of the *Helsinki Declaration* of 1975 and the Committee on Human Experimentation of Shanghai Jiao Tong University.

### Immunohistochemistry

Immunohistochemistry was performed as described previously (Fu et al., 2016). Briefly, paraffin sections were deparaffinized with xylene and washed with 100% ethanol (EtOH), 95% EtOH, 75% EtOH, 50% EtOH, and phosphate-buffered saline (PBS). Sections were then treated with 10 mM of either a pH 6.0 sodium citrate solution or pH 9.0 Tris-ethylenediaminetetraacetic acid antigen retrieval solution in a microwave at high power for 5 minutes to reach boiling point, followed by low power for a further 15 minutes. The sections were allowed to naturally cool down to room temperature (approximately 20–25°C). The slides were then blocked with Tris-buffered saline with 0.1% Tween and 3% bovine serum albumin solution for 1 hour at room temperature. After blocking, the samples were incubated with primary antibodies at room temperature for 2 hours, followed by five washes of Tris-buffered saline with 0.1% Tween. Subsequently, the samples were incubated with fluorescent secondary antibodies overnight at 4°C. The treated samples were washed again with Tris-buffered saline with 0.1% Tween five times on the second day and mounted with PBS + 50% glycerol supplemented with Hoechst nuclear dye (1 μg/mL; Sigma-Aldrich, St. Louis, MO, USA, B2261), ready for imaging. Immunohistochemistry without primary antibodies was used as a negative control. All experiments were repeated to verify the reproducibility of the results. The following primary antibodies and dilutions were used: Aβ (1:200, Abcam, Cambridge, UK, Cat# ab201061, RRID: AB_2722492), Aβ/AβPP (1:200, CST, Danvers, MA, USA, Cat# 2450, RRID: AB_490857), phos-tau (1:200, Abcam, Cat# ab151559, RRID: AB_2893278), microtubule associated protein 2 (MAP2; 1:200, Proteintech, Rosemont, IL, USA, Cat# 17490-1-AP, RRID: AB_2137880), apolipoprotein E (ApoE; 1:200, Abcam, Cat# ab183597, RRID: AB_3331650), Sortilin1 (1:200, Abcam, Cat# ab263864, RRID: AB_2884942), alpha-hemoglobin (HBA; 1:200, Abcam, Cat# ab92492, RRID: AB_10561594), Cathepsin D (1:200, Abcam, Cat# ab75852, RRID: AB_1523267), lysosome-associated membrane protein 2 (Lamp2; 1:100, Proteintech, Cat# 66301-1-Ig, RRID: AB_2881684), Cathepsin D (1:100, Proteintech, Cat# 66534-1-Ig, RRID: AB_2881897), glycosylated hemoglobin type A1C (HbA1c; 1:100, OkayBio, Nanjing, Jiangsu, China, Cat# K5a2), hemin (1:100, Absolute Antibody, Redcar, UK, Cat# 1D3), advanced glycation end products (AGE; 1:200, Abcam, Cat# ab23722, RRID: AB_447638), collagen type IV (ColIV; 1:200, Abcam, Cat# ab236640), and smooth muscle actin alpha 2 (ACTA2; 1:400, Proteintech, Cat# 23081-1-AP, RRID: AB_2815024). We used the following secondary antibodies and dilutions: donkey anti-mouse Alexa Fluor 594 secondary antibody (1:400, Jackson ImmunoResearch, West Grove, PA, USA, Cat# 715-585-150, RRID: AB_2340854), donkey anti-rabbit Alexa Fluor 488 secondary antibody (1:400, Jackson ImmunoResearch, Cat# 711-545-152, RRID: AB_2313584), donkey anti-rabbit Alexa Fluor 594 secondary antibody (1:400, Jackson ImmunoResearch, Cat# 711-585-152, RRID: AB_2340621), and donkey anti-mouse Alexa Fluor 488 secondary antibody (1:400, Jackson ImmunoResearch, Cat# 715-545-150, RRID: AB_2340846).

### Rhodanine staining

Rhodanine staining was performed as described previously (Fu et al., 2023). Briefly, paraffin sections were first deparaffinized as described above. After a quick wash in 95% ethanol, the slides were stained with rhodanine staining solution (0.01% p-dimethylaminobenzalrhodanine; Baso Diagnostics Inc., Zhuhai, China, BA4346) and incubated at 37°C for 30 minutes. After staining, the slides were quickly washed in 95% ethanol, followed by washing in water five times, and then mounted with PBS + 50% glycerol solution for imaging analysis.

### Alizarin red staining

Paraffin sections were deparaffinized as described above. The slides were stained in the Alizarin red staining solution (2% Alizarin red, pH 4.2, Beyotime Biotechnology, Shanghai, China, C0138) for 5 minutes at room temperature. After staining, the sections were washed five times with water and mounted with PBS + 50% glycerol solution for imaging.

### Imaging and morphometry analysis

Fluorescent images were captured with a CQ1 confocal fluorescent microscope (Yokogawa, Ishikawa, Japan), and the color images of sections with histological stains were acquired with an Olympus IX71 fluorescent microscope (Olympus Co., Tokyo, Japan). Exposure settings for imaging axonal staining and senile plaque staining are distinct. To image axonal Aβ staining clearly, the exposure time needs to be increased significantly. The blue autofluorescence of senile plaques and axons (MetaBlue) was imaged with a standard 4′,6-diamidino-2-phenylindole (DAPI) blue fluorescence channel using the CQ1 confocal microscope at an excitation wavelength of 405 nm and an emission spectrum of 447–460 nm. Images were then analyzed with the ImageJ software (version 1.54f; National Institutes of Health, Bethesda, MD, USA) (Schneider et al., 2012). When comparing signal intensities with the same exposure settings, we used the mean area density parameter to define marker densities. The perimeter of enlarged AD axons in the transverse orientation was measured to simplify axon diameter estimation using the formula: diameter = perimeter/3.14. The diameter of control brain axons was measured directly using the ImageJ line tool with the microscopy scale as a reference.

### Colocalization analysis

Quantitation of the colocalization of paired markers was performed using the ImageJ "Colocalization Threshold" plugin. The area of interest (e.g., a senile plaque, axon, dystrophic neurite, or specific cell) was selected with a small rectangle. To increase the sensitivity of the analysis, the object of interest was further defined via a freehand region of interest selection. Paired RGB images from two different fluorescent channels were converted into 16-bit images and analyzed using the "Colocalization Threshold" plugin with the selected region of interest. The quantitation of colocalization was reported as M1 after threshold (tM1) or tM2 for the two respective markers. A merged picture highlighting the colocalized pixels was also produced using the software.

### Statistical analysis

All data were subjected to the Shapiro–Wilk normality test using the SPSS Statistics 19 software (IBM Corp., Armonk, NY, USA). Two-tailed unpaired *t*-tests were used to compare means of normally distributed data in Excel 2007 (Microsoft, Redmond, WA, USA). For non-normally distributed data, we used the nonparametric Mann-Whitney *U* test to compare means using the SPSS Statistics 19 software. Spearman correlation analysis in SPSS Statistics 19 was used to examine correlations. A $P < 0.05$ was considered significant.

## Results

### Axon amyloidosis and enlargement in Alzheimer's disease brain tissues

In our previous work, we detected Aβ staining in senile plaques, cerebral amyloid angiopathy, neurons, and red blood cells (Fu et al., 2023, 2024). After careful re-examination of the Aβ staining patterns of AD brain sections under optimized staining conditions and longer exposure settings, we observed clear axon-specific Aβ staining patterns that were not detected previously (two overview images of Aβ staining of AD tissue axons in longitudinal and transverse orientations are provided in **Additional Figures 1** and **2**). In the current study, we focused primarily on axon fragments in the gray matter or at the gray matter/white matter boundary, which may be defined as proximal axons that are close to the neuronal soma. We extended the analysis to axons in the white matter because many aspects of white matter axon fragments showed similar changes as the proximal axons. **Figure 1A** and **Additional Figures 1** and **2** show that axon amyloidosis was widespread in

AD brain tissues. Aβ immunostaining was distributed along the entire length of numerous axons. Aβ-positive axons were observed around senile plaques and in regions without senile plaques in the vicinity. Axonal amyloidosis was detected in axons in both longitudinal and transverse orientations. Furthermore, axons with Aβ staining were often observed as grouped clusters, which corresponded to the well-documented human cortical structural character of "axon bundles." Axon bundles, also known as "axonal tracts" (van Groen et al., 2014; Katsuki and Hijioka, 2017), were frequently observed in Layer VI of the cerebral cortex, which comprises the gray matter/white matter formation boundary. An image of MAP2-labeled axon bundles in the control brain is shown in **Additional Figure 3**. According to the literature, "axon bundles" derived from the neurons are the only neural cell process type that exhibits a "bundling" phenotype, different from astrocytic or microglial processes. These intracortical axon bundles had an average transverse diameter of 61.61 ± 9.88 μm ($n$ = 11). Each bundle contained an average of 19.09 ± 4.61 axons ($n$ = 11; **Additional Figure 3**). The enlarged and often bundled axons, but not unaffected axons, in AD brain tissues could be clearly identified via phase contrast microscopy owing to the enhanced contrast and darker appearance. These enlarged axons were not labeled with ionized calcium-binding adaptor molecule 1 (Iba1), a microglial marker, or glial fibrillary acidic protein (GFAP), an astrocyte marker (**Additional Figure 4**). Additionally, the enlarged axons could be identified with amyloid blue autofluorescence, an alternative marker of amyloidosis to Aβ antibody staining (Dowson, 1981; Gao et al., 2019), which we have previously referred to as "MetaBlue" (Fu et al., 2023, 2024). Blue autofluorescence is an intrinsic characteristic of Aβ homo- or hetero-oligomerization and is not abolished by copper sulfate quenching treatment. From cortical surface to white matter, we observed axon bundles at both transverse and longitudinal orientations within the same pathological section, which indicated different axon bundle populations (**Additional Figures 1–3**). Axon bundles were most clearly observed in Layer VI of the cortex, characterized by long axon fragments that bundled together.

Puff-like spheroid formations were detected in a subset of Aβ-positive axons. Spheroids often form in regions with further-enhanced Aβ staining. Aβ-positive axons exhibit a general enlargement phenotype (**Figure 1B**), which is a basic characteristic that appears more frequently than spheroid formation. We measured the diameters of Aβ-positive axons in the transverse orientation outside of senile plaque regions because the strong plaque Aβ staining precluded accurate identification of Aβ-positive axons within senile plaques. These Aβ-positive proximal axons had an average diameter of 1.94 ± 0.59 μm ($n$ = 200), whereas MAP2-labeled proximal axons from control frontal lobe samples measured 1.13 ± 0.39 μm ($n$ = 34). Therefore, Aβ-positive axon diameters were 1.72 ± 0.52 fold larger than control axons (Mann-Whitney $U$ test, $P$ < 0.001). In addition, among the AD tissue axon samples, the mean Aβ staining intensity was weakly positively correlated with axon diameter (Spearman $r$ = 0.338, $P$ < 0.001, $n$ = 200; **Additional Figure 5**), which further emphasizes the positive influence of Aβ on axonal enlargement. When axons in the white matter were analyzed, MetaBlue-positive amyloid-laden axon diameters were 3.80 ± 0.69 μm ($n$ = 100), which indicated even greater enlargement than proximal axons in the gray matter or at the gray matter/white matter boundary. Our data suggest that Aβ-amyloidosis-associated axonal enlargement is a basic pathological phenotype of AD.

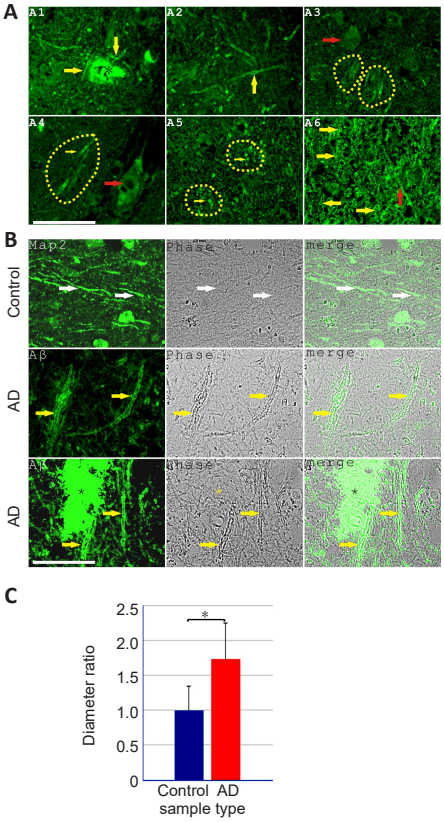


**Figure 1 | Axon amyloidosis and enlargement are important pathological phenotypes in AD.**

(A) Axon amyloidosis was detected in AD frontal lobe tissues with the Aβ antibody with green fluorescence (Alexa Fluor 488). (A1) Aβ expression was detected in both a senile plaque (indicated by an asterisk) and axons (indicated by arrows). (A2) An axon at the longitudinal orientation showed spheroid formations with Aβ expression (indicated by an arrow). (A3) Two clusters of Aβ-positive axons in the longitudinal direction (indicated by dashed lines) were observed, indicating Aβ staining of axon bundles. An Aβ-containing neural cell is indicated by a red arrow. (A4) A cluster of Aβ-positive axons in the longitudinal direction (indicated by dashed lines) was detected. Blood vessel lumen Aβ expression is indicated by a red arrow. An axon with clear Aβ-staining is indicated by a yellow arrow. (A5) Two clusters of Aβ-positive axons in the transverse direction (indicated by dashed lines) were observed. Individual axons are indicated by yellow arrows. (A6) Axons with abundant axonal Aβ staining (mostly in the transverse direction; yellow arrows) were observed in the white matter. One longitudinal axon is indicated by a red arrow. Scale bar: 50 μm. (B) A general enlargement of axons in AD brain tissues was observed when comparing control axons (indicated by white arrows, top panel) marked by MAP2 antibody staining (green, Alexa Fluor 488) and amyloid-loaded axons in AD (indicated by yellow arrows, bottom two panels) marked by Aβ immunostaining (green, Alexa Fluor 488). A senile plaque in the bottom panel is labeled with an asterisk. Scale bar: 50 μm. (C) Imaging measurements showed that Aβ-positive axons ($n$ = 200) were 1.72 ± 0.52 fold larger than control axons ($n$ = 34; *$P$ < 0.001, Mann–Whitney $U$ test). AD: Alzheimer's disease; Aβ: amyloid-β; Map2: microtubule associated protein 2.

**Axons of patients with Alzheimer's disease show a reduction in structural protein MAP2**

To examine the effect of axon amyloidosis on neurons, brain sections of AD patients were stained with an antibody against MAP2, a microtubule-associated structural protein highly expressed in the neuronal soma, dendrite, and axon. Immunostaining of the AD and control brain sections showed strong MAP2 staining of the neuronal soma and axons and clear expression in the Layer VI axon bundles and white matter axons (**Figures 1** and **2** and **Additional Figure 3**). This demonstrates that MAP2 is a useful marker for axons in human brain pathology studies. **Figure 2A** (top panel) shows that there were significantly fewer signals of MAP2-stained axons (i.e., MAP2-positive axon numbers decreased by more than half, with a reduction rate of 53.8%, when examining from the longitudinal orientation). Moreover, counting from the transverse orientation, we observed an even larger reduction of 79.8% in axon MAP2 signals (bottom panel of **Figure 2A**). Double immunostaining with an Aβ antibody showed that MAP2 expression correlated inversely with Aβ staining in AD tissue axons (**Figure 2B**). In the white matter tissue of AD patients, many axons exhibited a decrease in MAP2 protein while bearing significant Aβ staining. MAP2 staining on Aβ-positive axons was often fragmented and diffuse. Typically, there is very little MAP2 immunostaining within dense-core senile plaques. We also observed reduced MAP2 expression in amyloid-laden axons in the white matter when we used amyloid blue autofluorescence as an axon amyloidosis marker (**Figure 2C**). We estimated that, on the basis of one set of experiments, Aβ immunohistochemistry labeled 44.2% of proximal axons (we counted the average number of Aβ-labeled axons per axon bundle at the transverse orientation [8.44 ± 4.10, $n$ = 16] and divided by the average axon bundle axon number of 19.09 in control samples obtained earlier). These data suggested that nearly half of all axons were affected by Aβ amyloidosis. Axons with amyloid blue autofluorescence showed much weaker MAP2 intensity (0.36 ± 0.07, $n$ = 100) than axons without amyloid blue autofluorescence ($n$ = 25). The amyloid-laden axons lost MAP2 expression at an average rate of 64% in white matter. Aside from the decrease in the MAP2 protein in axons, we observed reduced MAP2 immunostaining intensity in the soma in neurons with intracellular Aβ (**Additional Figure 6**), which suggests that Aβ has a deleterious effect on MAP2 expression in both axons and cell bodies.

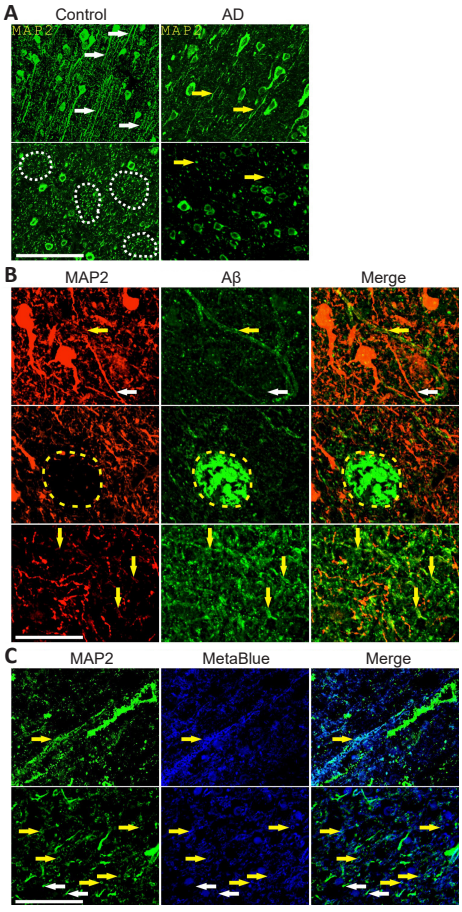


**Figure 2** | **Axons in AD frontal brain tissues show a decrease in axonal structural protein MAP2.**

(A) At longitudinal (top panel) and transverse orientations (bottom panel), significantly fewer MAP2-positive axons were observed in AD brain tissues compared with control brain tissues. The top panel shows that there were 26 long MAP2-positive axon fragments (representative axons are indicated by white arrows) in the control sample and only 12 long MAP2-positive axon fragments (indicated by yellow arrows) in the AD sample, indicating 53.8% fewer MAP2-positive axons in AD patient samples. The bottom panel shows that there were 391 strong MAP2-positive axon dots (those with an axon bundle formation are indicated by white dashed lines) in the control frontal lobe tissue sample and 79 strong MAP2-positive axon dots (representative dots are indicated by yellow arrows) in the AD frontal lobe tissue sample, which indicates 79.8% fewer MAP2-positive axon signals in AD samples. Scale bar: 100 µm. (B) Three representative images show the correlation between the decrease in axonal MAP2 signals and the increase in Aβ immunostaining in axons of AD brain tissues. The top two images show axons in the gray matter with greatly reduced MAP2 staining (Aβ-laden axons are indicated by yellow arrows and the unaffected axons are indicated by white arrows). The yellow dashed lines in the second image surround a dense-core senile plaque with barely detectable MAP2 immunostaining. The bottom image shows numerous Aβ-loaded axons with diminished MAP2 staining in the white matter. Scale bar: 50 µm. (C) Two representative images show greatly reduced axonal MAP2 staining in Aβ-laden axons labeled with amyloid blue autofluorescence in the white matter. The top panel shows axons primarily in the longitudinal direction, and the bottom panel shows axons primarily in the transverse direction. The yellow arrows indicate the Aβ-loaded axons and the white arrows indicate the control axons without blue autofluorescence. Axons with amyloid blue autofluorescence showed much weaker MAP2 intensity (0.36 ± 0.07, $n$ = 100) compared with axons without amyloid blue autofluorescence ($n$ = 25). Scale bar: 50 µm. AD: Alzheimer's disease; Aβ: amyloid-β; Map2: microtubule associated protein 2.

### Detection of lysosomal destabilization in Alzheimer's disease frontal lobe tissues

We hypothesized that the decrease in the MAP2 protein in axons was due to faulty protein degradation events, although other mechanisms, such as MAP2 messenger RNA transcription reduction or protein synthesis deficiency, are also possible. Lysosome and proteasome pathways are major pathways of protein degradation. Because we observed that Aβ-positive axons appeared to contain many vesicles, we stained the sections with a lysosomal enzyme marker Cathepsin D. Although we previously identified weak extracellular Cathepsin D staining codistributing with senile plaque Aβ aggregates, we also observed clear intracellular neuronal lysosome Cathepsin D staining (Fu et al., 2023). However, neuronal Cathepsin D staining was not homogeneous. Rather, abnormal Cathepsin D staining was observed frequently in senile plaque regions (**Figure 3A–C**). Normal lysosomal staining showed granule-like patterns with strong Cathepsin D signals. By contrast, in senile plaques, 71.2% ± 9.6% ($n$ = 10) of Cathepsin D staining resided in lysosomal compartments showing abnormal Cathepsin D staining with enlarged, diffuse, and weak staining patterns, which indicated lysosomal destabilization, as reported previously (Takahashi et al., 2002; Liu et al., 2010; Zaretsky et al., 2022). We did observe a weak yet detectable Aβ staining in these abnormal lysosomal compartments. The lysosomal compartments (including all Cathepsin D-labeled compartments) within the senile plaques measured 4.32 ± 1.99 µm ($n$ = 122) in size, which was 3.65 ± 1.68 times larger (Mann–Whitney $U$ test, $P$ < 0.001) than the control lysosomes outside of plaque regions (1.18 ± 0.39 µm, $n$ = 60); moreover, these were characterized by considerably weaker Cathepsin D staining intensity (0.76 ± 0.3; Mann–Whitney $U$ test, $P$ < 0.001). In AD tissue axons, Aβ and lysosomal enzyme marker Cathepsin D were highly colocalized with a tM1 value (for Aβ) of (0.852 ± 0.106, $n$ = 8), indicating the predominant presence of axonal Aβ in the lysosomes. We also detected diffuse and weak Cathepsin D staining patterns along the length of Aβ-positive axons, which suggested the occurrence of axonal lysosome destabilization (**Figure 3D–F**). Control cellular lysosomes distant from senile plaques had primarily strong, clear, and granule-like Cathepsin D staining patterns (**Figure 3G**). Additional evidence showing axonal amyloidosis associated with unusually diffuse Cathepsin D staining is presented in **Additional Figure 7**, where we used amyloid blue autofluorescence as an amyloidosis marker. However, lysosome destabilization was not limited to axons. On closer inspection of the intracellular lysosomes, many neural cells also revealed heterogeneous Cathepsin D staining patterns (**Figure 4**). In summary, the destabilized lysosomes may be related to a decrease in the MAP2 protein in axons in patients with AD.

Lysosomes are abundant in the neuronal soma. If lysosome destabilization occurs in regions surrounding senile plaques, we would expect to also detect destabilized lysosomes in cell bodies. Indeed, we observed frequent lysosomal destabilization in Aβ-containing neural cells (**Figure 4** and **Additional Figure 8**). We use lysosomes from neural cells with limited Aβ staining as internal controls for unaffected lysosomes (**Figure 4A**). The control lysosomes appeared normal-looking with punctuate and compact staining of Cathepsin D. In cells with abundant Aβ signals, lysosomes became enlarged and clustered, and their Cathepsin D staining became diffuse. The enlargement of lysosomes filled with Aβ could be observed at the single lysosome level (yellow arrows in **Figure 4B** and **C**). Furthermore, the Aβ-loaded and enlarged lysosomes often clustered together to form large lysosomal domains with diffuse Cathepsin D staining (**Figure 4D** and **E**). Quantitation showed that 71.8% ± 13.8% (seven cells measured) of intracellular Aβ colocalized with Cathepsin D staining, which suggested that the majority of intracellular Aβ was in the lysosomes or destabilized lysosomes. The Aβ-containing lysosomes ($n$ = 30) had an average size of 1.63 ± 0.27 µm, which was 2.23 ± 0.38 times as large ($P$ < 0.001, $t$-test) and 0.32 ± 0.12 times of Cathepsin D intensity ($P$ < 0.001, Mann–Whitney $U$ test) as the control lysosomes with no Aβ staining (average size: 0.73 ± 0.09 µm, $n$ = 12), which demonstrated that Aβ-associated lysosome destabilization is a distinctive phenotype of intracellular amyloidosis. The enlargement, clustering, and destabilization of Aβ-containing lysosomes may be related to the axonal enlargement observed in AD brain tissues. Aβ staining was also occasionally detected at extra-lysosomal locations in the cytoplasm and even the nucleus. We also observed occasional Cathepsin D staining in the nucleus (**Figure 4F** and **G**). The existence of Aβ and Cathepsin D in locations other than lysosomes may be related to lysosome destabilization and leakage; theoretically, in such conditions, lysosomal contents may be relocated to other cellular compartments. **Additional Figure 9** shows the comparison between AD and non-AD neural cell lysosomes, again demonstrating the phenomenon of lysosome destabilization in AD neural cells.

The above result further supports lysosome destabilization in AD as reported consistently in previous studies (Liu et al., 2010; Gowrishankar et al., 2015; Lee et al., 2022b; Zaretsky et al., 2022). However, whether abnormal lysosomes produce Aβ or Aβ induces lysosomal destabilization remains unclear. This complex question can be addressed by studying molecules that interact with Aβ. Previously, we established a link between Aβ senile plaque formation and intravascular hemolysis, vascular degeneration, and microaneurysm rupture (Fu et al., 2023, 2024). The relationship between microhemorrhage

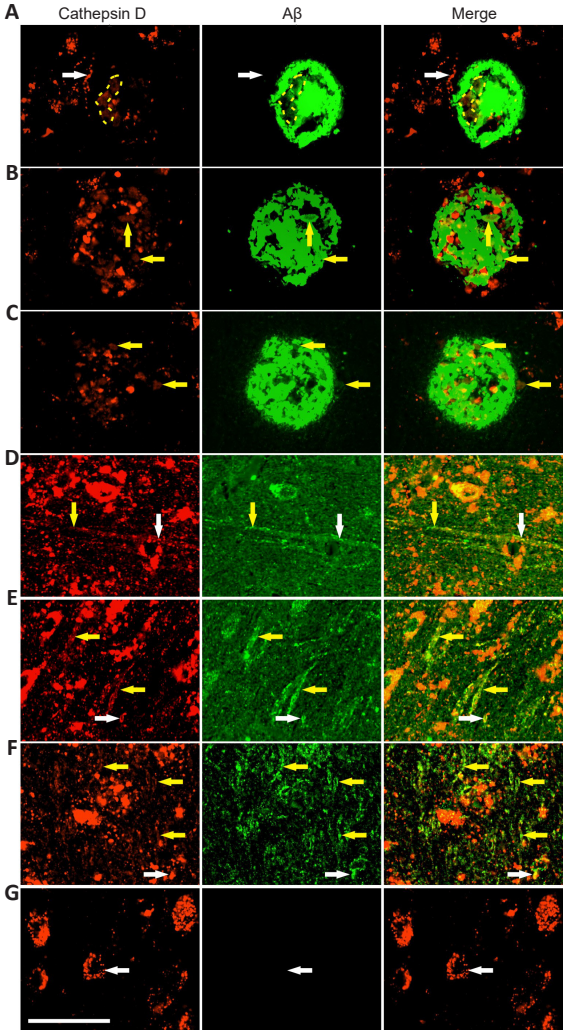


**Figure 3** | **Lysosomal destabilization is common in AD frontal lobe tissues.**
(A–C) Three representative plaques associated with lysosome destabilization. The top plaque was a typical dense-core plaque, whereas the bottom two plaques were more diffuse. All three plaques were associated with enlarged and diffuse Cathepsin D staining (red, Alexa Fluor 594) patterns (yellow dashed lines or yellow arrows), which is a characteristic of lysosome destabilization and lysosome permeabilization that is in contrast to the typical, granule-like strong lysosome staining with focal Cathepsin D positivity (indicated by white arrows in the top panel). Quantitation showed that 71.2% ± 9.6% ($n$ = 10) of Cathepsin D staining in the senile plaque regions located in lysosomal compartments displayed abnormal diffusive patterns. Weak Aβ staining (green, Alexa Fluor 488) was observed in these abnormal lysosomal compartments. (D–F) Three representative images illustrating diffuse Cathepsin D staining (red, Alexa Fluor 594) in the Aβ-positive axons (green, Alexa Fluor 488; indicated by yellow arrows). Simultaneously, colocalization between Aβ and Cathepsin D in lysosomes was abundant (indicated by white arrows). These three images were acquired using longer exposure settings than other images to show the weak axonal Aβ and Cathepsin D staining. (G) Intracellular lysosomes distant from amyloid plaques showed mostly clear, strong, and granule-like lysosomal Cathepsin D staining (red, Alexa Fluor 594, indicated by white arrows). Scale bar: 50 μm. AD: Alzheimer's disease; Aβ: amyloid-β.

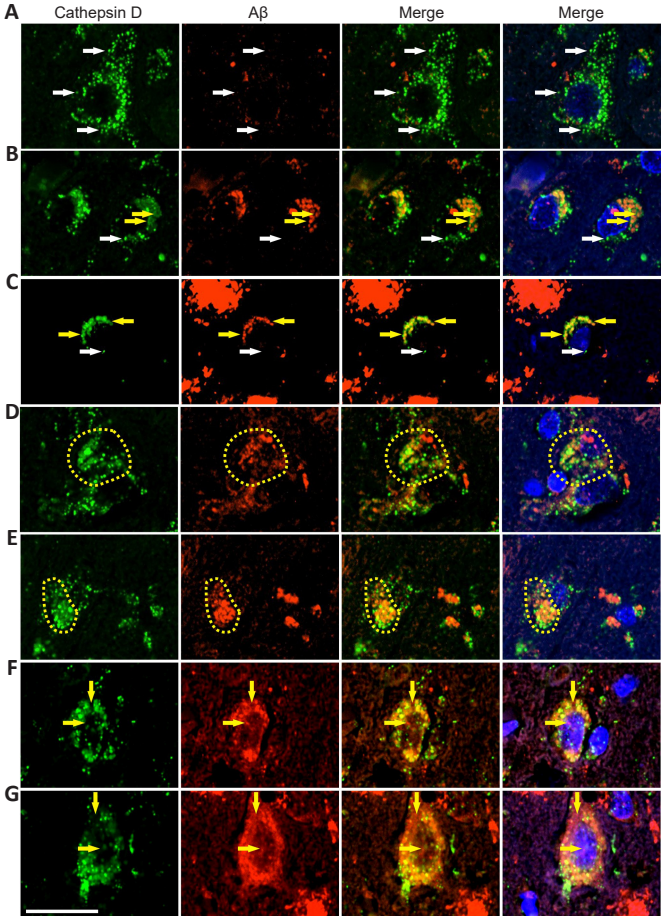


**Figure 4** | **Lysosomal destabilization is strongly associated with Aβ in the cell bodies of neural cells in AD frontal lobe tissues.**
(A) A control neural cell with little Aβ staining (red, Alexa Fluor 594) showed mostly normal lysosome Cathepsin D staining (green, Alexa Fluor 488) patterns (indicated by white arrows). (B, C) Intracellular Aβ (red, Alexa Fluor 594) was associated with lysosome destabilization, which could be identified at the single lysosome level by significant lysosome enlargement and diffuse staining (indicated by yellow arrows), whereas control lysosomes (indicated by white arrows) showed compact and bright Cathepsin D staining (green, Alexa Fluor 488). (D, E) Two representative images indicating that intracellular Aβ expression was associated with lysosome enlargement, clustering, and diffuse staining. The dashed boxes highlight the areas enriched for both Aβ staining and lysosomal destabilization. (F, G) Two representative images of neural cells containing not only lysosomal Aβ (red, Alexa Fluor 594) and Cathepsin D (green, Alexa Fluor 488) but also extra-lysosomal cytoplasmic Aβ, nuclear Aβ, and nuclear Cathepsin D. Vertical arrows indicate cytoplasmic Aβ staining outside of Cathepsin D-stained areas and horizontal arrows indicate nuclear Aβ and Cathepsin D staining. Scale bar: 25 μm. AD: Alzheimer's disease; Aβ: amyloid-β.

and Aβ senile plaque formation has also been explored by others (Miyakawa et al., 1982; Cullen et al., 2005, 2006; Stone, 2008; Chuang et al., 2012; Bu et al., 2018; Hecht et al., 2018). Thus, Aβ may interact either directly or indirectly with hemolysis or vascular markers, which would be reflected in the co-distribution of Aβ with hemolytic or vascular markers. We analyzed the intracellular co-expression of a hemolysis-related marker HBA and two vascular-related markers ACTA2 and ColIV with Aβ (**Figure 5**). All three markers showed good colocalization with intracellular Aβ in lysosome-like structures. HBA and ACTA2 signals, as well as Aβ signals, were also frequently observed in the nucleus (**Figure 5A–C**). Quantitative analysis showed that HBA, ACTA2, and ColIV colocalized with Aβ at rates of 82.3% ± 17.6% ($n$ = 5), 78.4% ± 32.9% ($n$ = 5), and 95.7% ± 8.0% ($n$ = 5), respectively. When we performed HBA and Cathepsin D double-immunostaining on AD frontal lobe sections (**Figure 5D**), we observed the co-distribution of HBA signals with destabilized lysosomes, as indicated by enlarged and clustered lysosome compartments and diffuse Cathepsin D staining. Quantitative analysis showed that 43.2% ± 15.3% ($n$ = 5) of intracellular HBA staining colocalized with Cathepsin D staining. These findings indicate that the protein partners that interact with Aβ (e.g., HBA) are also associated with lysosome destabilization in neural cells.

### Destabilized lysosomes exist in dystrophic neurites in patients with Alzheimer's disease

The results above clearly showed that there is a lysosome destabilization phenotype associated with intracellular Aβ in the neuronal cells in AD. Because we focused mainly on the axonal phenotype of AD in this study, to further verify whether destabilized lysosomes are linked to axonal degeneration, we stained the tissue sections with a phos-tau antibody, a well-known axonal dystrophy marker in AD, and Lamp2, a lysosomal membrane marker. We observed the localization of abnormally diffuse lysosomal Lamp2 staining in phos-tau-positive dystrophic neurites, neurofibrillary tangles, axons, and neuropil threads (**Figure 6A**). Quantitative colocalization analysis showed that 45.4% ± 17.8% ($n$ = 6) of Lamp2 staining colocalized with phos-tau staining in the senile plaque dystrophic neurites, whereas 62.9% ± 22.3% ($n$ = 7) of Lamp2 staining colocalized with phos-tau staining in the neuropil

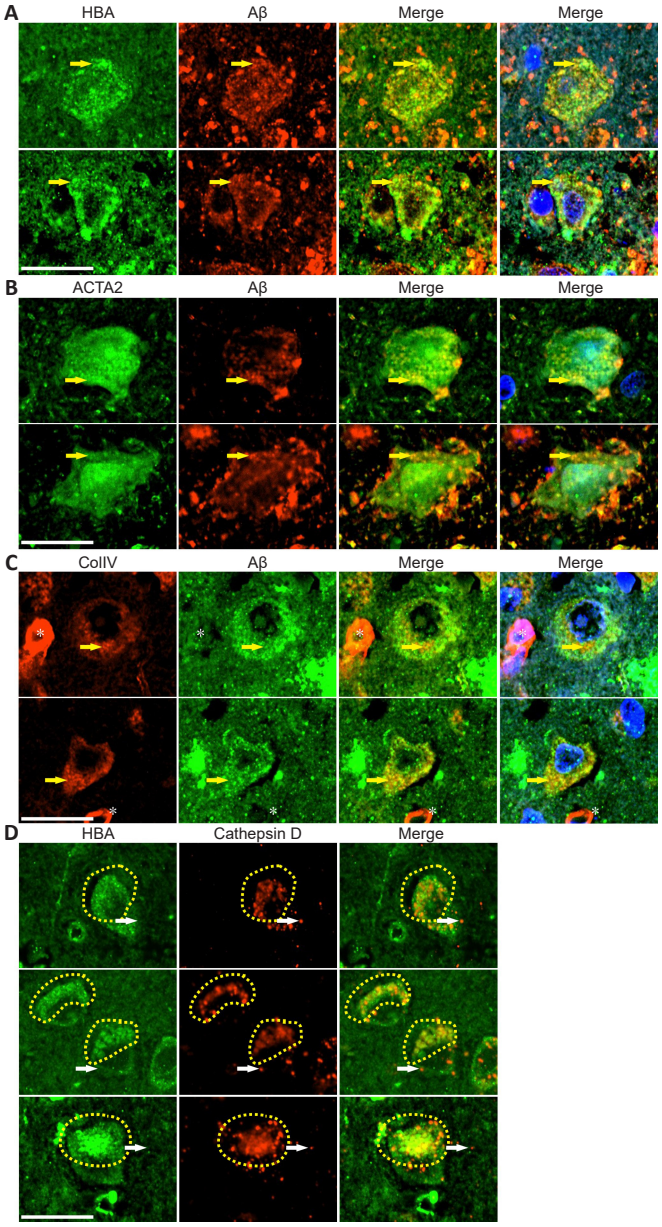


**Figure 5 | Blood and vascular proteins co-exist with intracellular Aβ in neural cells in AD frontal lobe tissues and may also be related to lysosome instability.**

(A) Representative images showing the co-expression of blood-related markers HBA (green, Alexa Fluor 488) and Aβ (red, Alexa Fluor 594). (B) Representative images showing the co-expression of vascular markers ACTA2 (green, Alexa Fluor 488) and Aβ (red, Alexa Fluor 594). (C) Representative images showing the co-expression of vascular markers ColIV (red, Alexa Fluor 594) and Aβ (green, Alexa Fluor 488). The colocalization of markers is indicated by yellow arrows. Two small blood vessels are indicated by asterisks in the ColIV staining panel. (D) Intracellular HBA (green, Alexa Fluor 488) expression domains overlapped with the region of lysosomal destabilization, which is indicated by enlarged and clustered lysosomal compartments and diffuse Cathepsin D staining (red, Alexa Fluor 594, marked with yellow dashed circles). Control HBA-unaffected lysosomes are indicated by white arrows. Scale bars: 25 µm. ACTA2: Smooth muscle actin alpha 2; AD: Alzheimer's disease; Aβ: amyloid-β; ColIV: collagen type IV; HBA: hemoglobin.

threads. Two additional images emphasizing the colocalization of Lamp2 and phos-tau staining in the dystrophic neurites in senile plaques are provided in **Additional Figure 10**. In addition, we detected an abundance of abnormally diffuse lysosomal Lamp2 staining in phos-tau-positive dystrophic axons in the white matter (**Figure 6A**, bottom panel). Neuropil thread is a collective term traditionally used for phos-tau staining in both axons and dendrites. We noticed that, throughout the brain, neuropil thread phos-tau staining was more abundant than phos-tau staining of tangles and senile plaque dystrophic neurites (**Additional Figure 11**). The phos-tau-positive neurites in AD tissues could be classified according to diameter as primary dystrophic neurites with an average diameter of 1.56 ± 0.37 µm ($n$ = 40) or secondary dystrophic neurites with an average diameter of 0.40 ± 0.09 µm ($N$ = 30), which may reflect the different size of axons and dendrites. When we stained the AD brain sections with both phos-tau and Aβ antibodies, we also detected colocalization between phos-tau and Aβ in dystrophic neurites, senile plaques, neurofibrillary tangles, neuropil threads, and axons (**Figure 6B**). Quantitative colocalization analysis showed that 34.4% ± 13.2% ($n$ = 6) of Aβ staining colocalized with phos-tau staining in the senile plaques. However, Aβ staining intensity in the dystrophic neurites, tangles, and axons was lower than that in the senile plaques. These data confirm that axonal dystrophy is linked to Aβ, tau phosphorylation, and lysosome destabilization.

### Axonal degeneration in Alzheimer's disease bears markers of hemorrhagic insults

Why cells and axons in AD brain tissues degenerate remains unclear. The mechanism of lysosome destabilization was initially proposed following cell culture studies (Liu et al., 2010; Zaretsky et al., 2022). However, *in vivo*, Aβ alone may not be solely responsible for the degeneration effect because Aβ interacts with numerous other proteins. Given our previous finding that senile plaques are formed by blood Aβ leakage into the brain upon microaneurysm rupture, we hypothesized that axonal damage in AD brain tissues is also associated with various blood-related proteins. Therefore, we examined axonal pathology using a variety of blood- and plasma-related markers. Results showed that enlarged axons in AD brains indeed carried blood and plasma markers, such as ApoE, HBA, HbA1C, and hemin (**Figure 7A–D**). Overt acute hemorrhage rarely surrounded these affected axons, which suggested that the intake of hemorrhagic markers in these axons is likely a chronic event. The presence of blood markers in axons is not dependent on the proximity to senile plaques. In addition, the distribution of hemorrhagic markers is not always quantitatively proportional to the intensity of Aβ in AD brain tissues; there can be even stronger staining of hemorrhagic markers in the axons than in the surrounding senile plaques, which is likely due to the differential enrichment or metabolism of amyloid protein complexes in axons *versus* senile plaques (an example is provided in the top panel of **Figure 7D** showing more hemin staining in the axons than in the adjacent senile plaque). Moreover, axon amyloidosis was associated with Sortilin1 expression, an endosomal/lysosomal marker (**Figure 7E**), which has also been implicated as a major receptor for ApoE and a component of senile plaques (Carlo et al., 2013; Hu et al., 2017). Quantitative colocalization analysis showed that, in the axons, ApoE, HBA, HbA1C, hemin, and Sortilin1 colocalized with Aβ at ratios of 97.1% ± 3.6% ($n$ = 12), 75.4% ± 9.5% ($n$ = 8), 88.9% ± 5.0% ($n$ = 8), 94.3% ± 9.9% ($n$ = 11), and 94.9% ± 5.0% ($n$ = 6), respectively. As shown in **Figure 3**, intracellular Aβ was predominantly detected in the lysosomes. Consistently, the above data suggest that intracellular ApoE, HBA, HbA1C, and hemin are also primarily located in the lysosomes. An overview image of widespread HBA and Aβ expression in the white matter axons is provided in **Additional Figure 12**. Additionally, when we stained the sections with red blood cell-related histological stains (e.g., Alizarin red and rhodanine) (Fu et al., 2023), many axons in the AD brain tissues were also positively stained (**Additional Figure 13**). In fact, the white matter tissue of AD brains was broadly stained with Alizarin red and rhodanine, similar to HBA, demonstrating a strong effect of hemorrhagic markers on the white matter axons. Taken together, these findings indicate that the axons were enriched for not only Aβ but also numerous hemorrhage-related markers.

### Axonal breakages are occasionally observed in Alzheimer's disease brain tissues

Whether axonal degeneration defects ultimately lead to axonal breakages in AD is a crucial question that needs addressing. We inspected hundreds of images containing Aβ-stained axons. Initially, we focused on axons inside senile plaques traveling in the longitudinal orientation because axons in the transverse orientation were difficult to identify individually. We observed that although many axons passing through the senile plaques were Aβ-positive and enlarged, they did not break (**Additional Figure 14**). However, we did find a few examples indicating that the axons were broken at locations outside of senile plaques. Using Aβ and AGE antibodies as markers for amyloidosis-affected axons, we were able to detect broken axons with gaps of up to 38.4 µm in width (**Figure 8A**). What caused these rare axonal breakages is not immediately clear. Additionally, we found that long stretches of amyloid-loaded vesicles with large spheroid formations on the axons caused marked dystrophy, to a degree that axon morphology could no longer be recognized (**Figure 8B**). The long stretch of clustering vesicles with spheroid formations was likely due to lysosome clustering, as indicated by the endosome/lysosomal marker Sortilin1 (**Figure 8C**). We speculate that in some cases, the continuous enlargement of destabilized lysosomal compartments across a long distance ultimately results in axonal breakages.

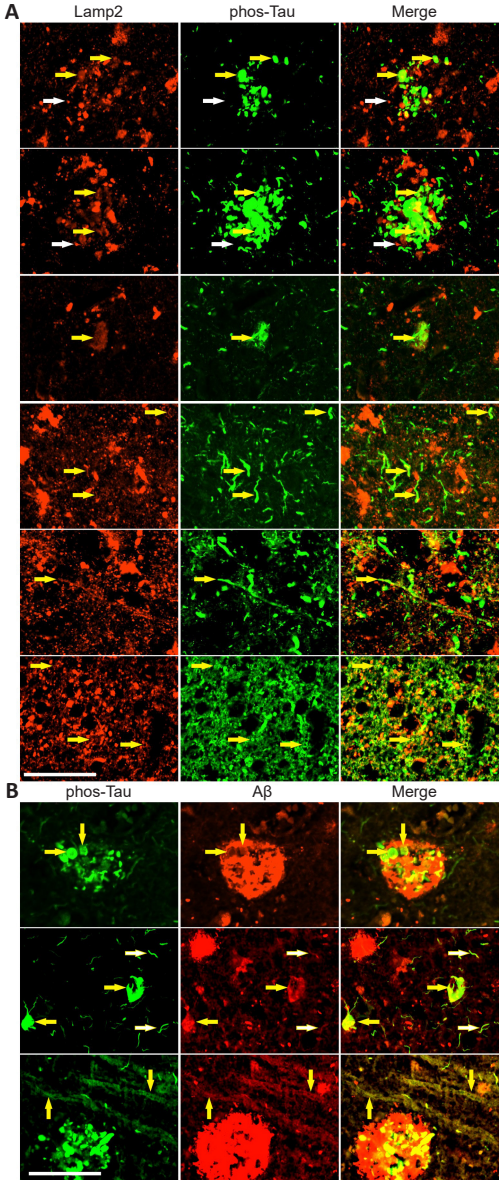


**Figure 6** | **Destabilized lysosomes are located in AD frontal lobe tissue dystrophic neurites, tangles, axons, and neuropil threads, and there was co-distribution between phos-tau and Aβ in dystrophic neurites, tangles, neuropil threads, and axons.**

(A) Abnormal lysosome Lamp2 staining (red, Alexa Fluor 594; indicated by yellow arrows) was detected in peri-plaque dystrophic neurites (top two panels), a representative tangle (third panel), neuropil threads (fourth panel), a representative longitudinal axon (fifth panel) and white matter axons (mostly in the transverse direction; bottom panel) marked with phos-tau immunostaining (green, Alexa Fluor 488). We observed long, diffuse, but relatively weak Lamp2 staining along the length of axons and neuropil threads, which highlights the intricacy of this defect. The bottom three images were acquired using longer exposure time settings to show the relatively weak signals in neuropil threads and axons. Control lysosomes not affected by tau phosphorylation are indicated by white arrows. Scale bar: 50 µm. (B) Phos-tau-positive (green, Alexa Fluor 488) dystrophic neurites (yellow arrows, top panel), tangles (yellow arrows), neuropil threads (white arrows; middle panel), and axons (yellow arrows, bottom panel) were also Aβ-positive (red, Alexa Fluor 594). Scale bar: 50 µm. AD: Alzheimer's disease; Aβ: amyloid-β.

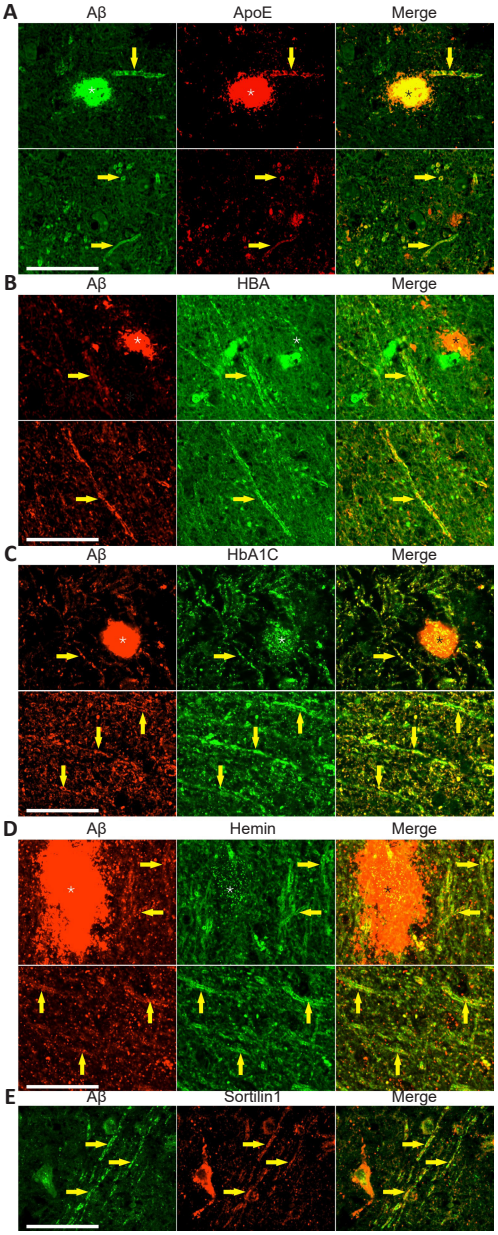


**Figure 7** | **Axon degeneration in AD bears the markers of hemorrhagic insults in AD frontal lobe tissues.**

(A–D) Four blood-related markers (ApoE, HBA, HbA1C, and hemin) all showed positivity in enlarged axons labeled with Aβ immunostaining. They were adjacent to senile plaques (top image in each panel) or not associated with senile plaques (bottom image in each panel). ApoE was stained red (Alexa Fluor 594), whereas HBA, HbA1C, and hemin were stained green (Alexa Fluor 488). Aβ was stained green (Alexa Fluor 488) in panel A and red (Alexa Fluor 594) in panels B–D. (E) Degenerating axons were positive for an endosomal/lysosomal marker Sortilin1 (red, Alexa Fluor 594). The affected axons are indicated by arrows and the senile plaques are indicated by asterisks. Scale bars: 50 µm. AD: Alzheimer's disease; ApoE: apolipoprotein E; Aβ: amyloid-β; HBA: hemoglobin; HbA1C: glycosylated hemoglobin type A1C.

## Discussion

Axonal amyloidosis induces additional axonal structural changes, such as a decrease in the MAP2 protein, which may be related to Aβ toxicity due to lysosomal destabilization. Whether MAP2 is an effective axon marker has been debated. MAP2 has been shown to label the neuronal cell soma, dendrites, and axons in hippocampal neuron culture and N2a cell line cell culture models (Dajas-Bailador et al., 2008; Pinatel et al., 2015). Furthermore, MAP2 is a good axon marker for pathological studies; for example, it has been applied successfully to rat brain traumatic axonal injury models (Li et al., 2016; Lee et al., 2022a; Liu et al., 2022). Some cell culture experiments in cultured dorsal root ganglion sensory neurons have claimed that MAP2 is a proximal-axon-restricted marker. However, careful inspection of the published data (Gumy et al., 2017) shows that MAP2 expression is not confined to proximal axons but extends along the length of axons. Quantitative colocalization analysis showed that nearly 71.8% of intracellular Aβ staining colocalized with Cathepsin D staining, which is strong evidence that lysosomes are the principal sites of intracellular amyloidosis. Studies have also shown *in vitro* that extracellular Aβ is taken up and concentrated in lysosomes and induces lysosome destabilization and permeabilization (Liu et al., 2010; Zaretsky et al., 2022). Intracellular lysosome acidification defects and lysosome permeabilization have been studied in mouse AD models and are considered a possible mechanism for neuronal cell death and senile plaque formation (Nixon et al., 2005; Lee et al., 2022b; Nixon, 2024). Additionally, a previous study identified abnormal protease-deficient lysosomes in swollen axons

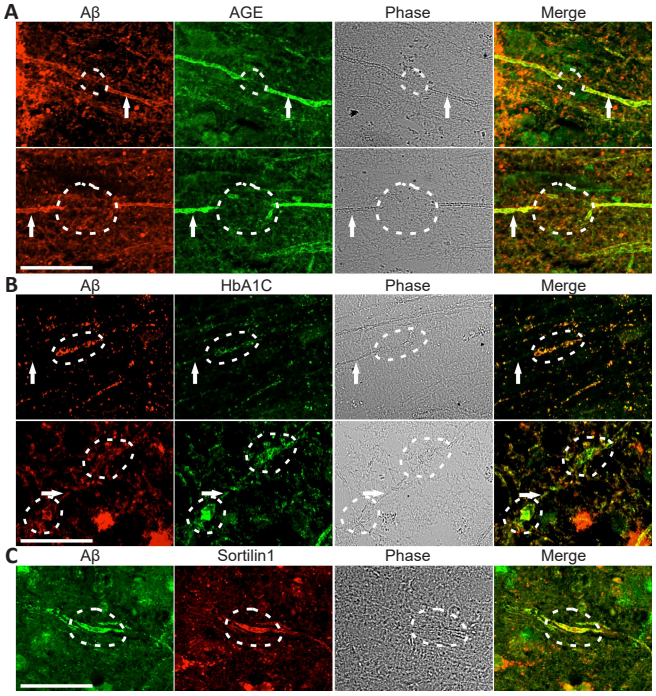


**Figure 8** | **Axonal breakages are occasionally observed in AD frontal lobe tissues.** (A) Two broken axons were identified with AGE (green, Alexa Fluor 488) and Aβ (red, Alexa Fluor 594) immunohistochemistry in AD brain tissues. The axonal gap in the top image measured 24.4 μm, whereas in the bottom image, it measured 38.4 μm. The broken regions are marked by dashed lines and the parental axons are indicated by arrows. (B) Two examples of damaged axons associated with large vesicle clusters and spheroid formation enriched for amyloid markers Aβ (red, Alexa Fluor 594) and HbA1C (green, Alexa Fluor 488). The long stretch of clustered vesicles (indicated by dashed lines) in the top panel measured 32.5 μm in length. The maximal width of the two large spheroids (indicated by dashed lines) in the bottom panel reached 6.2 μm (top-right position) and 8.3 μm (bottom-left position), respectively. The affected axons are indicated by arrows. (C) A long axonal region (indicated by dashed lines) with large spheroid formations associated with endosomal/lysosomal domains marked with Sortilin1 immunostaining (red, Alexa Fluor 594). This region measured 26.1 μm in length. The maximal width of the spheroid formation measured 4.1 μm. Scale bars: 50 μm. AD: Alzheimer's disease; AGE: advanced glycation end products; Aβ: amyloid-β; HbA1C: glycosylated hemoglobin type A1C.

surrounding senile plaques (Gowrishankar et al., 2015), and this lysosome defect was defined as a lysosome maturation deficiency. In this study, we provided evidence that Aβ is linked to lysosome destabilization at single lysosome and single axon levels. Moreover, we comprehensively analyzed axonal enlargement defects, particularly in intracortical axon bundles, which are rarely discussed in previous studies. Most importantly, we speculate that the axonal and cellular lysosomes were not intrinsically protease-deficient but were destabilized by Aβ and Aβ-associated hemorrhagic or vascular factors, such as ApoE, hemin, HbA1C, HBA, ACTA2, and ColIV. Aβ-associated factors very likely affect lysosome stability, maturation, or lysosome pH, as well as Aβ itself. Our findings further support previous evidence suggesting that the pathological Aβ peptide in AD neurons is derived from an exogenous source (i.e., hemorrhagic Aβ leakage) rather than from the neurons themselves (Cullen et al., 2006; Stone, 2008; Chuang et al., 2012; Bu et al., 2018; Fu et al., 2023, 2024). Although severe lysosome leakage may result in neuronal cell death, lysosome leakage in the cells could illicit a complex "lysosome leakage response" to counteract the damaging effect of lysosome leakage. Our preliminary data did not confirm a straightforward increase in neuronal apoptosis using a terminal deoxynucleotidyl transferase deoxyuridine triphosphate nick end labeling assay as an apoptotic marker and MAP2 reduction as a marker for lysosome leakage-associated neuronal proteomic damage. In addition, senile plaques with flower-like Cathepsin D-positive structures wrapped around dense-core amyloid blue fluorescence could not be confirmed as central-nucleated neurons with defective lysosomes because there was no nuclear staining in the plaque core when the blue autofluorescence was subtracted (Fu et al., 2024). Thus, more extensive investigations on the mechanism of the "lysosome leakage response" are warranted.

We believe that Aβ can be classified as a type of lysosomal "toxin," which exerts its unique toxicity upon lysosomal intake and processing. Our findings suggested that lysosomal destabilization is not due to Aβ alone but it is also related to Aβ-associated factors. For example, it is well established that hemin is a neurotoxic molecule itself, and lysosomes are a primary site for hemin metabolism (Robinson et al., 2009; Dang et al., 2011). Axonal amyloidosis is also associated with Sortilin1 expression. Sortilin1 is an endosome/lysosome marker that has been identified as a major receptor of ApoE (Carlo et al., 2013), whereas ApoE is a major binding protein of Aβ. Axons may take up exogenous Aβ complexes via receptor-related mechanisms, independent of or in conjunction with the neural soma, by the relay chains starting from Aβ, to ApoE, and finally to Sortilin1. The intake of a large number of hemorrhagic proteins alongside Aβ could induce severe axonal proteostatic stress, in addition to the toxicity effects of Aβ, especially when the axon–soma connection is compromised.

Both Aβ deposition and tau phosphorylation are important components of AD pathology. However, the relationship between these two events is unclear. It has previously been suggested that Aβ and tau colocalize in AD "synaptosomes" (Fein et al., 2008). Our quantitative imaging analysis provided an alternative mechanism that Aβ and tau are both connected to destabilized lysosomes. We found that 71.2% of Cathepsin D staining in senile plaque regions was located in destabilized lysosomal compartments. In the neural soma with significant Aβ staining, 75.5% of intracellular lysosomes were in destabilized forms marked by diffuse Cathepsin D staining. Furthermore, 45.4% of Lamp2 lysosomal marker staining colocalized with phos-tau-stained neuritic dystrophy in senile plaques, whereas 62.9% of Lamp2 staining colocalized with phos-tau staining in neuropil threads with largely diffuse Lamp2 patterns. These results provide robust evidence that destabilized lysosomes connect key pathologies of AD: senile plaque formation, intracellular amyloidosis, and neuritic dystrophy with tau phosphorylation.

Numerous studies show that Aβ endocytosis induces lysosome destabilization (Takahashi et al., 2002; Liu et al., 2010; Tam et al., 2014); moreover, there is strong evidence that Aβ induces tau phosphorylation (Zheng et al., 2002; Mattsson-Carlgren et al., 2020). In this study, tau phosphorylation was associated with destabilized lysosomes in tangles, dystrophic neurites, neuropil threads, and axons. It remains unknown whether tau phosphorylation or lysosome destabilization is the upstream event. Our data showed that MAP2, a tau-related microtubule-binding protein, was reduced significantly (i.e., > 50% loss based on our estimate) in Aβ-laden axons. If we consider lysosome destabilization and MAP2 reduction in axons and previous evidence that MAP2 competes with tau for microtubule binding (Sandoval and Vandekerckhove, 1981) and may prevent tau aggregation (Holden et al., 2023), lysosomal destabilization may work upstream of tau phosphorylation by chronically degrading its competitive inhibitor MAP2. Therefore, the biological significance of lysosome destabilization in the neuronal soma in AD brain tissues is worthy of future investigation.

Owing to the limited supply of AD brain tissue specimens, we were unable to compare the severity of axonal amyloidosis defects or intracellular lysosomal destabilization across different Braak stages. Nevertheless, axonal breakages were observed in a small number of axons. When axonal breakages occur and are not repaired, Wallerian degeneration of axons may occur, which can result in axonal loss. Because axonal breakages with small gaps are difficult to detect, the true number of axonal breakage events in AD brains may be higher than that observed. Thus, further studies are needed to understand the frequency of axonal breakages and Wallerian degeneration in AD brains. A previous *in vitro* study using hippocampal neuron cell culture models showed that the Aβ peptide induces axonal degeneration that precedes cell death (Alobuia et al., 2013), which indicates a possible "dying back" mechanism of neuronal degeneration in AD. Our data similarly indicated that axonal degeneration is an important early step of AD pathogenesis. It is well established that both Wallerian degeneration and axonal degeneration are affected by various genetic mutations (Coleman and Freeman, 2010; Neumann et al., 2011; Teoh et al., 2018; Wang et al., 2024). To combat AD effectively, we must develop methods that prevent microvascular blood leakage and axonal accumulation of Aβ and hemorrhagic proteins. Treatments that can specifically slow Wallerian degeneration and facilitate axonal repair, reconnection, and regeneration would also likely be beneficial for AD patients. Currently, several Food and Drug Administration-approved Aβ-targeted monoclonal antibody

drugs to reduce Aβ-burdens in AD patients are available in the clinic, such as lecanemab and donanemab antibodies (Terao and Kodama, 2024; Arroyo-Pacheco et al., 2025). However, effective drugs for AD must demonstrate to the public that they can significantly lower intracellular toxic Aβ levels to reduce axonal damage.

**Acknowledgments:** *We want to thank the help from Dr. Ma Chao and Dr. Qiu Wenying for providing AD tissue sections from National Human Brain Bank for Development and Function, Chinese Academy of Medical Sciences and Peking Union Medical College, Beijing, China. Additionally, we want to thank Dr. Ming Yang from Shanghai Jiao Tong University, Dr. Xiangli Zhang from Shandong University, Dr. Peng Du and Dr. Lei Xia from Xinhua Hospital for valuable scientific discussions. Moreover, we want to thank Housheng Wang, Pingxin Liu, Xiaoyi Bao, and Jun Wang from Shanghai Jiao Tong University for their excellent laboratory assistance. This study was supported by the Institute of Basic Medical Sciences, Chinese Academy of Medical Sciences, Neuroscience Center, and the China Human Brain Banking Consortium.*

**Author contributions:** *HF conceived the study, designed and supervised the experiments and wrote the manuscript; HF and JL performed the experiments; HF, JL, CZ, GG, QG, XG, and DC did the data analysis. All authors reviewed the manuscript and approved the final version of the manuscript.*

**Conflicts of interest:** *All authors declare no conflicts of interest.*

**Author statement:** *An earlier version of this paper has been posted as a preprint on bioRxiv with doi: https://doi.org/10.1101/2024.06.10.598057, which is available from: https://www.biorxiv.org/content/10.1101/2024.06.10.598057v2.full.pdf.*

**Data availability statement:** *All data relevant to the study are included in the article or uploaded as Additional files.*



**Additional files:**

***Additional Figure 1:*** *An overview of Aβ expressing in longitudinal axon bundles, senile plaques, CAA blood vessel walls, the blood vessel lumen and also neurons in AD frontal brain tissues.*

***Additional Figure 2:*** *An overview on many axon bundles with Aβ-positive axons in a transverse orientation in AD frontal brain tissues.*

***Additional Figure 3:*** *MAP2 antibody labels intracortical axon bundles clearly in control frontal brain tissues.*

***Additional Figure 4:*** *Enlarged axons in AD frontal brain tissues are not stained with microglial marker Iba1 or astroglia marker GFAP although contacts between microglial cells or astrocytes and these axons are observed.*

***Additional Figure 5:*** *Spearman correlation of mean Aβ staining intensity and axon diameter.*

***Additional Figure 6:*** *Intracellular Aβ associates with the decrease of MAP2 expression in neurons in AD frontal brain tissues.*

***Additional Figure 7:*** *Axon amyloidosis is associated with fragmented, very diffusive staining of lysosome marker Cathepsin D in AD frontal brain tissues.*

***Additional Figure 8:*** *A representative overview on Aβ and Cathepsin D expression in neural cells in AD frontal brain tissues.*

***Additional Figure 9:*** *Lysosomes in AD frontal brain tissues show signs of destabilization with lysosome clustering, enlargement and diffusive Cathepsin D staining in comparison to clear granule-looking lysosomes from control brain tissues of non-AD samples.*

***Additional Figure 10:*** *The colocalization of phos-tau and Lamp2 immunostaining in the dystrophic neurites in frontal brain tissues of AD.*

***Additional Figure 11:*** *tau phosphorylation antibody stained abundant dystrophic neurites are widely distributed in AD frontal brain tissues, not restricted to dystrophic neurites surrounding the senile plaques and tangled neurons.*

***Additional Figure 12:*** *An overview image of HBA and Aβ staining in AD frontal brain sections shows abundant HBA accumulation in the brain white matter axons.*

***Additional Figure 13:*** *Many axons are positively stained by Alizarin Red or Rhodanine in AD frontal brain tissues.*

***Additional Figure 14:*** *Enlarged axons are detected inside of senile plaques in AD frontal brain tissues but axon breakage was not readily observed.*

## References

Alobuia WM, Xia W, Vohra BP (2013) Axon degeneration is key component of neuronal death in amyloid-β toxicity. Neurochem Int 63:782-789.

Arroyo-Pacheco N, Sarmiento-Blanco S, Vergara-Cadavid G, Castro-Leones M, Contreras-Puentes N (2025) Monoclonal therapy with lecanemab in the treatment of mild Alzheimer's disease: a systematic review and meta-analysis. Ageing Res Rev 104:102620.

Blazquez-Llorca L, Valero-Freitag S, Rodrigues EF, Merchán-Pérez Á, Rodríguez JR, Dorostkar MM, DeFelipe J, Herms J (2017) High plasticity of axonal pathology in Alzheimer's disease mouse models. Acta Neuropathol Commun 5:14.

Braak H, Del Tredici K (2013) Amyloid-β may be released from non-junctional varicosities of axons generated from abnormal tau-containing brainstem nuclei in sporadic Alzheimer's disease: a hypothesis. Acta Neuropathol 126:303-306.

Bu XL, et al. (2018) Blood-derived amyloid-β protein induces Alzheimer's disease pathologies. Mol Psychiatry 23:1948-1956.

Carlo AS, Gustafsen C, Mastrobuoni G, Nielsen MS, Burgert T, Hartl D, Rohe M, Nykjaer A, Herz J, Heeren J, Kempa S, Petersen CM, Willnow TE (2013) The pro-neurotrophin receptor sortilin is a major neuronal apolipoprotein E receptor for catabolism of amyloid-β peptide in the brain. J Neurosci 33:358-370.

Chen Y, Wang Y, Song Z, Fan Y, Gao T, Tang X (2023) Abnormal white matter changes in Alzheimer's disease based on diffusion tensor imaging: A systematic review. Ageing Res Rev 87:101911.

Chuang JY, Lee CW, Shih YH, Yang T, Yu L, Kuo YM (2012) Interactions between amyloid-β and hemoglobin: implications for amyloid plaque formation in Alzheimer's disease. PLoS One 7:e33120.

Coleman MP, Freeman MR (2010) Wallerian degeneration, Wld(S), and Nmnat. Annu Rev Neurosci 33:245-267.

Cras P, Kawai M, Lowery D, Gonzalez-DeWhitt P, Greenberg B, Perry G (1991) Senile plaque neurites in Alzheimer disease accumulate amyloid precursor protein. Proc Natl Acad Sci U S A 88:7552-7556.

Cullen KM, Kócsi Z, Stone J (2005) Pericapillary haem-rich deposits: evidence for microhaemorrhages in aging human cerebral cortex. J Cereb Blood Flow Metab 25:1656-1667.

Cullen KM, Kócsi Z, Stone J (2006) Microvascular pathology in the aging human brain: evidence that senile plaques are sites of microhaemorrhages. Neurobiol Aging 27:1786-1796.

Dajas-Bailador F, Jones EV, Whitmarsh AJ (2008) The JIP1 scaffold protein regulates axonal development in cortical neurons. Curr Biol 18:221-226.

Dang TN, Robinson SR, Dringen R, Bishop GM (2011) Uptake, metabolism and toxicity of hemin in cultured neurons. Neurochem Int 58:804-811.

Dowson JH (1981) A sensitive method for the demonstration of senile plaques in the dementing brain. Histopathology 5:305-310.

Fan Q, Tian Q, Ohringer NA, Nummenmaa A, Witzel T, Tobyne SM, Klawiter EC, Mekkaoui C, Rosen BR, Wald LL, Salat DH, Huang SY (2019) Age-related alterations in axonal microstructure in the corpus callosum measured by high-gradient diffusion MRI. Neuroimage 191:325-336.

Fein JA, Sokolow S, Miller CA, Vinters HV, Yang F, Cole GM, Gylys KH (2008) Co-localization of amyloid beta and tau pathology in Alzheimer's disease synaptosomes. Am J Pathol 172:1683-1692.

Fellgiebel A, Yakushev I (2011) Diffusion tensor imaging of the hippocampus in MCI and early Alzheimer's disease. J Alzheimers Dis 26 Suppl 3:257-262.

Fu H, Ma Y, Yang M, Zhang C, Huang H, Xia Y, Lu L, Jin W, Cui D (2016) Persisting and increasing neutrophil infiltration associates with gastric carcinogenesis and e-cadherin downregulation. Sci Rep 6:29762.

Fu H, Li J, Du P, Jin W, Gao G, Cui D (2023) Senile plaques in Alzheimer's disease arise from Aβ- and Cathepsin D-enriched mixtures leaking out during intravascular haemolysis and microaneurysm rupture. FEBS Lett 597:1007-1040.

Fu H, Li J, Zhang C, Du P, Gao G, Ge Q, Guan X, Cui D (2024) Aβ-aggregation-generated blue autofluorescence illuminates senile plaques as well as complex blood and vascular pathologies in Alzheimer's disease. Neurosci Bull 40:1115-1126.

Gao Y, Liu Q, Xu L, Zheng N, He X, Xu F (2019) Imaging and spectral characteristics of amyloid plaque autofluorescence in brain slices from the APP/PS1 mouse model of Alzheimer's disease. Neurosci Bull 35:1126-1137.

Gelman S, Palma J, Ghavami A (2020) Axonal conduction velocity in CA1 area of hippocampus is reduced in mouse models of Alzheimer's disease. J Alzheimers Dis 77:1383-1388.

Gowrishankar S, Yuan P, Wu Y, Schrag M, Paradise S, Grutzendler J, De Camilli P, Ferguson SM (2015) Massive accumulation of luminal protease-deficient axonal lysosomes at Alzheimer's disease amyloid plaques. Proc Natl Acad Sci U S A 112:E3699-3708.

Gumy LF, Katrukha EA, Grigoriev I, Jaarsma D, Kapitein LC, Akhmanova A, Hoogenraad CC (2017) MAP2 defines a pre-axonal filtering zone to regulate KIF1- versus KIF5-dependent cargo transport in sensory neurons. Neuron 94:347-362.e347.

Hardy JA, Higgins GA (1992) Alzheimer's disease: the amyloid cascade hypothesis. Science 256:184-185.

Hartline DK, Colman DR (2007) Rapid conduction and the evolution of giant axons and myelinated fibers. Curr Biol 17:R29-35.

Hecht M, Krämer LM, von Arnim CAF, Otto M, Thal DR (2018) Capillary cerebral amyloid angiopathy in Alzheimer's disease: association with allocortical/hippocampal microinfarcts and cognitive decline. Acta Neuropathol 135:681-694.

Holden MR, Krzesinski BJ, Weismiller HA, Shady JR, Margittai M (2023) MAP2 caps tau fibrils and inhibits aggregation. J Biol Chem 299:104891.

Hu X, Hu ZL, Li Z, Ruan CS, Qiu WY, Pan A, Li CQ, Cai Y, Shen L, Chu Y, Tang BS, Cai H, Zhou XF, Ma C, Yan XX (2017) Sortilin fragments deposit at senile plaques in human cerebrum. Front Neuroanat 11:45.

Katsuki H, Hijioka M (2017) Intracerebral hemorrhage as an axonal tract injury disorder with inflammatory reactions. Biol Pharm Bull 40:564-568.

Kolaric KV, Thomson G, Edgar JM, Brown AM (2013) Focal axonal swellings and associated ultrastructural changes attenuate conduction velocity in central nervous system axons: a computer modeling study. Physiol Rep 1:e00059.

Lane CA, Hardy J, Schott JM (2018) Alzheimer's disease. Eur J Neurol 25:59-70.

Lee EJ, Hong SK, Choi DH, Gum SI, Hwang MY, Kim DS, Oh JW, Lee ES (2022a) Three-dimensional visualization of cerebral blood vessels and neural changes in thick ischemic rat brain slices using tissue clearing. Sci Rep 12:15897.

Lee JH, Yang DS, Goulbourne CN, Im E, Stavrides P, Pensalfini A, Chan H, Bouchet-Marquis C, Bleiwas C, Berg MJ, Huo C, Peddy J, Pawlik M, Levy E, Rao M, Staufenbiel M, Nixon RA (2022b) Faulty autolysosome acidification in Alzheimer's disease mouse models induces autophagic build-up of Aβ in neurons, yielding senile plaques. Nat Neurosci 25:688-701.

Li R, Ma K, Zhao H, Feng Z, Yang Y, Ge H, Zhang X, Tang J, Yin Y, Liu X, Tan L, Feng H (2016) Cattle encephalon glycoside and ignotin reduced white matter injury and prevented post-hemorrhagic hydrocephalus in a rat model of intracerebral hemorrhage. Sci Rep 6:35923.

Liu RQ, Zhou QH, Ji SR, Zhou Q, Feng D, Wu Y, Sui SF (2010) Membrane localization of beta-amyloid 1-42 in lysosomes: a possible mechanism for lysosome labilization. J Biol Chem 285:19986-19996.

Liu XY, Chang ZH, Chen C, Liang J, Shi JX, Fan X, Shao Q, Meng WW, Wang JJ, Li XH (2022) 3D printing of injury-preconditioned secretome/collagen/heparan sulfate scaffolds for neurological recovery after traumatic brain injury in rats. Stem Cell Res Ther 13:525.

Mattsson-Carlgren N, Andersson E, Janelidze S, Ossenkoppele R, Insel P, Strandberg O, Zetterberg H, Rosen HJ, Rabinovici G, Chai X, Blennow K, Dage JL, Stomrud E, Smith R, Palmqvist S, Hansson O (2020) Aβ deposition is associated with increases in soluble and phosphorylated tau that precede a positive Tau PET in Alzheimer's disease. Sci Adv 6:eaaz2387.

Miyakawa T, Shimoji A, Kuramoto R, Higuchi Y (1982) The relationship between senile plaques and cerebral blood vessels in Alzheimer's disease and senile dementia. Morphological mechanism of senile plaque production. Virchows Arch B Cell Pathol Incl Mol Pathol 40:121-129.

Neumann B, Nguyen KC, Hall DH, Ben-Yakar A, Hilliard MA (2011) Axonal regeneration proceeds through specific axonal fusion in transected C. elegans neurons. Dev Dyn 240:1365-1372.

Nixon RA, Wegiel J, Kumar A, Yu WH, Peterhoff C, Cataldo A, Cuervo AM (2005) Extensive involvement of autophagy in Alzheimer disease: An immuno-electron microscopy study. J Neuropathol Exp Neurol 64:113-122.

Nixon RA (2024) Autophagy-lysosomal-associated neuronal death in neurodegenerative disease. Acta Neuropathol 148:42.

Parandavar E, Shafizadeh M, Ahmadian S, Javan M (2024) Long-term demyelination and aging-associated changes in mice corpus callosum; evidence for the role of accelerated aging in remyelination failure in a mouse model of multiple sclerosis. Aging Cell 23:e14211.

Pinatel D, Hivert B, Boucraut J, Saint-Martin M, Rogemond V, Zoupi L, Karagogeos D, Honnorat J, Faivre-Sarrailh C (2015) Inhibitory axons are targeted in hippocampal cell culture by anti-Caspr2 autoantibodies associated with limbic encephalitis. Front Cell Neurosci 9:265.

Qian X, Yue L, Mellor D, Robbins NM, Li W, Xiao S (2022) Reduced peripheral nerve conduction velocity is associated with Alzheimer's disease: a cross-sectional study from China. Neuropsychiatr Dis Treat 18:231-242.

Robinson SR, Dang TN, Dringen R, Bishop GM (2009) Hemin toxicity: a preventable source of brain damage following hemorrhagic stroke. Redox Rep 14:228-235.

Salvadores N, Gerónimo-Olvera C, Court FA (2020) Axonal degeneration in AD: The contribution of Aβ and tau. Front Aging Neurosci 12:581767.

Sandoval IV, Vandekerckhove JS (1981) A comparative study of the in vitro polymerization of tubulin in the presence of the microtubule-associated proteins MAP2 and tau. J Biol Chem 256:8795-8800.

Schneider CA, Rasband WS, Eliceiri KW (2012) NIH Image to ImageJ: 25 years of image analysis. Nat Methods 9:671-675.

Stone J (2008) What initiates the formation of senile plaques? The origin of Alzheimer-like dementias in capillary haemorrhages. Med Hypotheses 71:347-359.

Takahashi RH, Milner TA, Li F, Nam EE, Edgar MA, Yamaguchi H, Beal MF, Xu H, Greengard P, Gouras GK (2002) Intraneuronal Alzheimer abeta42 accumulates in multivesicular bodies and is associated with synaptic pathology. Am J Pathol 161:1869-1879.

Tam JH, Seah C, Pasternak SH (2014) The Amyloid Precursor Protein is rapidly transported from the Golgi apparatus to the lysosome and where it is processed into beta-amyloid. Mol Brain 7:54.

Teoh JS, Wong MY, Vijayaraghavan T, Neumann B (2018) Bridging the gap: axonal fusion drives rapid functional recovery of the nervous system. Neural Regen Res 13:591-594.

Terao I, Kodama W (2024) Comparative efficacy, tolerability and acceptability of donanemab, lecanemab, aducanumab and lithium on cognitive function in mild cognitive impairment and Alzheimer's disease: A systematic review and network meta-analysis. Ageing Res Rev 94:102203.

Tsai J, Grutzendler J, Duff K, Gan WB (2004) Fibrillar amyloid deposition leads to local synaptic abnormalities and breakage of neuronal branches. Nat Neurosci 7:1181-1183.

van Groen T, Miettinen P, Kadish I (2014) Axonal tract tracing for delineating interacting brain regions: implications for Alzheimer's disease-associated memory. Future Neurol 9:89-98.

Wang P, Shao Y, Al-Nusaif M, Zhang J, Yang H, Yang Y, Kim K, Li S, Liu C, Cai H, Le W (2024) Pathological characteristics of axons and alterations of proteomic and lipidomic profiles in midbrain dopaminergic neurodegeneration induced by WDR45-deficiency. Mol Neurodegener 19:62.

Yuan P, Zhang M, Tong L, Morse TM, McDougal RA, Ding H, Chan D, Cai Y, Grutzendler J (2022) PLD3 affects axonal spheroids and network defects in Alzheimer's disease. Nature 612:328-337.

Zaretsky DV, Zaretskaia MV, Molkov YI (2022) Membrane channel hypothesis of lysosomal permeabilization by beta-amyloid. Neurosci Lett 770:136338.

Zheng WH, Bastianetto S, Mennicken F, Ma W, Kar S (2002) Amyloid beta peptide induces tau phosphorylation and loss of cholinergic neurons in rat primary septal cultures. Neuroscience 115:201-211.

*C-Editor: Zhao M; S-Editors: Yu J, Li CH; L-Editors: Iwabuchi S, Yu J, Song LP; T-Editor: Jia Y*

**与淀粉样变性、溶酶体不稳定和出血相关的病理性轴突增大是阿尔茨海默病的主要缺陷**
**文章特色分析**

一、文章重要性

1. 揭示 AD 中轴突病变的核心地位

传统上 AD 研究多集中于神经元胞体（如神经纤维缠结）和突触（如突触丢失），而该研究首次系统性地提出轴突淀粉样变性、轴突肿大、溶酶体不稳定和微出血是 AD 病理的重要组成部分，并强调轴突损伤是 AD 神经功能衰退的关键因素之一。

2. 连接血管病变与神经退行性变

文章提出出血性淀粉样变性是 AD 病理的核心环节，将血管源性 Aβ 渗漏、血红蛋白等血液蛋白的摄入与轴突内溶酶体不稳定联系起来，为理解 AD 中血管因素与神经退行之间的关系提供了新视角。

3. 提出轴突传导速度下降的结构基础

研究指出轴突肿大和球状体形成会减缓动作电位传导速度，这为解释 AD 患者认知功能下降提供了潜在的神经电生理机制。

二、创新性特色

1. 首次系统描述 AD 中轴突肿大与 Aβ 沉积的关系
   - 发现 Aβ 阳性轴突直径平均为对照组的 1.72 倍。
   - 轴突肿大与 MAP2 蛋白减少、tau 磷酸化、溶酶体 destabilization 密切相关。
2. 揭示溶酶体不稳定在 AD 轴突病变中的核心作用
   - 发现 Aβ 主要位于溶酶体中，且 Aβ 阳性溶酶体体积是对照的 2.23 倍。
   - 溶酶体 destabilization 不仅发生在轴突，也见于神经元胞体。
3. 提出“出血-溶酶体-轴突”病理轴
   - 发现轴突内存在多种血液蛋白（如 ApoE、血红蛋白、HbA1C、血红素），提示慢性微出血是 AD 轴突病变的重要诱因。
   - 这些蛋白与 Aβ 共定位，可能加剧溶酶体负担和不稳定。
4. 观察到罕见的轴突断裂现象
   - 发现轴突断裂并推测其可能导致 Wallerian 变性，进一步加剧神经连接丧失。

三、对学科的启示

1. 拓展 AD 病理机制的认识

研究将 AD 从传统的“Aβ 斑块与 tau 缠结”二元模型扩展为多系统病变模型，强调轴突、溶酶体和血管因素的交互作用。

2. 提示新的治疗靶点
   - 针对溶酶体稳定性的治疗策略可能有助于减缓轴突病变。
   - 控制微血管渗漏和血液蛋白入脑可能成为 AD 干预的新方向。
3. 推动 AD 早期诊断标志物的开发

轴突肿大、溶酶体 destabilization 和血液蛋白沉积可能成为影像学或体液生物标志物，用于早期识别 AD 病理进程。

4. 强调轴突保护在 AD 治疗中的重要性

未来 AD 治疗不应仅关注清除 Aβ 或抑制 tau，还应包括保护轴突完整性、促进轴突再生的策略。

总结

该研究通过多组化、免疫荧光和共定位分析，系统揭示了 AD 中轴突病变的病理特征及其与溶酶体不稳定、微出血的密切联系，具有概念创新、机制深入、临床转化潜力大的特点，为理解 AD 的全病程病理机制提供了重要补充，也为开发新型治疗策略奠定了理论基础。